Clim Dyn
DOI 10.1007/s00382-008-0432-4

An analysis on observed and simulated PNA associated atmospheric diabatic heating

B. Yu · Y. M. Tang · X. B. Zhang · A. Niitsoo

Received: 31 January 2008 / Accepted: 3 June 2008

Abstract This study examines the PNA associated atmospheric diabatic heating by linearly isolating the influence of ENSO. The analysis is based on the NCEP–NCAR and ERA-40 reanalyses and a 1,000-year-long integration of the CCCma coupled climate model. Both the vertically integrated and three-dimensional diabatic heating are examined. The Rossby wave sources in association with the PNA are also diagnosed. The PNA-related heating is confined outside the tropics and is dominated by anomalies in the eastern Pacific, with a north–south dipole structure in mid-latitudes and the northern subtropics. The heating anomalies change sign with height in mid-latitudes but have the same sign throughout the troposphere in the northern subtropics. Relatively weak heating anomalies also appear in mid-latitudes, downstream of the heating dipole over North America and the western North Atlantic. The heating anomalies are largely supported by the advections related to the mean state throughout the troposphere, and partially damped by the advections related to the eddy effect, particularly at the upper troposphere over the North Pacific. Broadly similar patterns are seen from the NCEP–NCAR and ERA-40 reanalyses. Yet anomalous heating centers are generally located at relatively lower troposphere for the ERA-40 with respect to the NCEP–NCAR. The tropical heating anomalies are rather weak, remarkably different from those related to ENSO variability. In addition, the Rossby wave source collocates with the atmospheric diabatic forcing in the mid-high latitudes over the PNA sector, and shows no forcing source in the tropics. The results demonstrate possible forcing in the mid-high latitudes, regardless of tropical heating for the PNA teleconnection. The modeled heating and wave forcing anomalies in association with the modeled PNA compare reasonably well with the reanalysis-based estimates, increasing confidence in the observational results. The analysis provides further evidence of the independence of the PNA on ENSO from the diabatic heating point of view.

Keywords Climate variability · PNA teleconnection · ENSO · Atmospheric diabatic heating

B. Yu (✉) · X. B. Zhang · A. Niitsoo
Climate Research Division, Environment Canada,
4905 Dufferin Street, Toronto, ON M3H 5T4, Canada
e-mail: bin.yu@ec.gc.ca

Y. M. Tang
Environmental Science and Engineering,
University of Northern British Columbia,
Prince George, BC, Canada

1 Introduction

The Pacific-North American (PNA) teleconnection pattern (Wallace and Gutzler 1981), indicated by a train of atmospheric waves arching from the tropical Pacific across North America, is one of the most prominent variability modes of the atmosphere and has been investigated extensively (e.g., Trenberth et al. 1998 for a review). Among those studies, one focus is on the excitation of this wave train by the atmospheric diabatic heating. In this aspect, more effort has been devoted to relating tropical heating to the lower boundary condition (e.g., Held et al. 2002, and references therein), especially the sea surface temperature (SST) anomalies of the most significant interannual El Niño-Southern Oscillation (ENSO) variability in the tropics. The PNA tends to be positive during El Niño events (e.g., Renwick and Wallace 1996). Nigam et al. (2000) showed that ENSO related diabatic heating

contains heating anomalies primarily in the central-eastern equatorial Pacific and cooling anomalies over the South Pacific convergence zone (SPCZ), the Maritime continent and the western North Pacific, in agreement with the ENSO precipitation anomalies reflecting rainfall reduction over the western Pacific and enhancement near the dateline (e.g., Wallace et al., 1998).

It has been suggested that ENSO related SST forcing can selectively amplify natural forms of internal variability, such as low-frequency variability of the mid-latitude atmosphere, but cannot generate new structures (e.g., Lau 1997; Palmer 1999, among others). Hoerling et al. (1997) demonstrated that the atmospheric response to ENSO forcing with noticeable nonlinearity, estimated by a summation of atmospheric responses to positive and negative ENSO states, primarily due to the differences in tropical diabatic forcing. On the other hand, it has also been proposed that climate variability in the PNA sector is not strongly related to ENSO (e.g., Deser and Blackmon 1995; Zhang et al. 1996). In particular, Straus and Shukla (2002, and references therein) concluded that ENSO-related SSTs force a circulation pattern quite distinct from the internally generated PNA mode.

In general, stationary wave anomalies (such as the PNA pattern) may be produced either by internally generated dynamical perturbations of the atmosphere or by external forcing. It is noted that substantial variability can arise in midlatitudes without external forcing as a result of internal nonlinear atmospheric dynamics (e.g., Zwiers 1987; Hartmann 1995). Nevertheless, external forcing may tend to favor the occurrence of certain types of variations (e.g., Trenberth et al. 1998). Studies have also shown that diabatic heating contributes substantially to divergence and large-scale atmospheric circulation anomalies in the tropics and mid-latitudes during ENSO events (e.g., Nigam et al. 2000; DeWeaver and Nigam 2004). Hence, it is useful to examine the atmospheric heating anomalies in association with the dynamical perturbations and forcing that are directly related to the PNA wave anomalies. A preliminary analysis was made recently by diagnosing both the three-dimensional (3D) and the vertically integrated atmospheric diabatic heating in association with the PNA pattern, based on the U.S. National Centers for Environmental Prediction–National Center for Atmospheric Research (NCEP–NCAR) reanalysis (Kistler et al. 2001) for the period from January 1949 to December 2003 (Yu 2007). It is found that the PNA related heating is dominated by anomalies in the eastern Pacific, with a north-south dipole structure in mid-latitudes and the northern subtropics. In contrast, the tropical heating anomalies are rather weak, remarkably different from those related to ENSO variability, and may be characterized by the heating nonlinearity with anomalies in the vicinity of the western Pacific. The study confirmed the distinct differences between the PNA and ENSO, consistent with Straus and Shukla (2002), from the diabatic heating viewpoint.

Two main issues will be addressed in this follow up study. One is relevant to the estimation of atmospheric diabatic heating using different datasets. An accurate specification of diabatic heating is vital for understanding both the atmospheric circulation and its variation. However, uncertainties and discrepancies exist in making this estimation (e.g., Sardeshmukh 1993) using different kinds of datasets. For instance, Trenberth et al. (2001) made comparisons and evaluations of the radiation and surface heat fluxes based on the NCEP–NCAR and ECMWF (the European Centre for Medium-Range Weather Forecasts) reanalyses. They found that non-trivial systematic differences exist between the two datasets. Figure 1 shows the geographical distribution of the December–February mean vertically integrated atmospheric diabatic heating for the NCEP–NCAR and the ERA-40 reanalyses and for their difference. The vertically integrated heating is estimated directly from the radiative fluxes at the top and the bottom of the atmosphere and the precipitation rate and turbulent heat fluxes at the surface (see more details later in Sect. 3.2). The heating patterns are broadly similar from the two reanalyses. Positive heating regions are generally located over summer hemisphere landmasses, with the intertropical convergence zone (ITCZ) extending across the Pacific, Atlantic and Indian oceans around 5–10°N and the SPCZ, and with the regions of the Kuroshio Current and Gulf Stream with extensions across the ocean basins at higher northern latitudes. Negative heating regions are primarily associated with cold surfaces and with polar regions, especially in the winter hemisphere. The heating anomalies extending over the Oceans in the extra-tropics are closely linked to the storm tracks. The main differences between the two reanalyses are seen in the tropics, particularly in the ITCZ and the SPCZ, and are dominated by precipitation differences (not shown). The discrepancy of the tropical heating between the two datasets raises one major concern regarding the results reported in Yu (2007), which will be addressed in this analysis by comparing results from both reanalyses. We will show below that the main results stay the same, only some modest differences are seen between the two. This may be because systematic errors and biases in the means from the two datasets are partially removed by the compositing process (e.g., WCRP 2000).

Another issue is relevant to the observational data length, based on the reanalyses that cover only the period in the late half of the twentieth century, and to potential quality problems of the data. As reported in previous studies (e.g., Nitta and Yamada 1989; Graham 1994; Trenberth and Hurrell 1994; among others), there is a

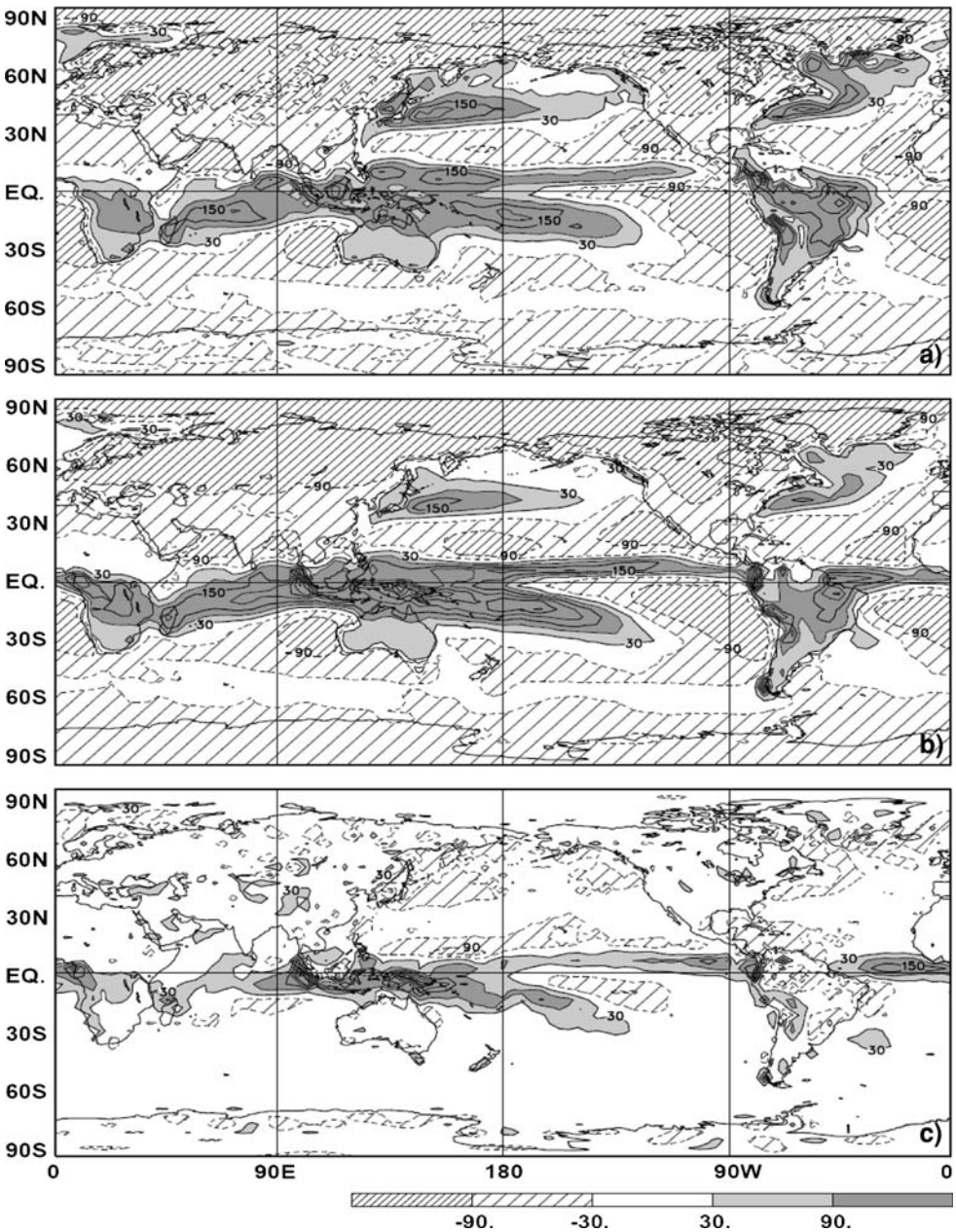

Fig. 1 Climatological patterns of December–February mean vertically integrated diabatic heating $\tilde{Q}$ for the NCEP–NCAR reanalysis (upper panel), the ERA-40 reanalysis (middle panel) and their difference (the ERA-40 minus the NCEP–NCAR, lower panel). Contour interval is 60.0 Wm^{-2} (…, −90.0, −30.0, 30.0, …), with the zero contour omitted

climate shift in the atmospheric circulation throughout the troposphere at around 1976. Considerable evidence has emerged of a substantial decadal change in the north Pacific atmosphere and ocean lasting from about 1976 to 1988. The long-term variation of climate may have an effect on some of the results obtained in Yu (2007) and on the observational results given below. In addition, large changes in the global atmospheric observing system in the 1970s (e.g., Bengtsson et al. 2004, among others), such as the introduction of satellite data in 1979, may also have an effect on some of our diagnostics with the reanalysis datasets. We attempt to address these concerns and to confirm the observational evidence by analyzing a 1,000-year-long climate simulation produced with the Canadian Center for Climate Modelling and Analysis (CCCma) coupled climate model.

Thus, the main purposes of this study are to further document the PNA associated atmospheric diabatic heating by linearly isolating the influence of ENSO. We will provide further evidence showing that the atmospheric heating related to the PNA and ENSO differs remarkably based on the NCEP–NCAR and ERA-40 reanalyses and a long coupled climate model integration, and explore the 3D characteristics of diabatic heating in association with the PNA. The rest of the paper is organized as follows. Section 2 describes the reanalyses and modeling data and the

diagnostic methods. Section 3 briefly discusses the relationship between the PNA and ENSO, and then presents the observational results of the vertically integrated diabatic heating, the 3D heating and the Rossby wave sources in association with the PNA after linearly removing the influence of ENSO. Section 4 provides some modeling evidence. A summary is given in Sect. 5.

2 Data and diagnostic methods

2.1 PNA and ENSO indices

The winter (December–February, DJF) mean PNA index defined in Wallace and Gutzler (1981), based on standardized 500-hPa geopotential height values in four centers of action, was obtained from http://jisao.washington.edu/data_sets/pna. ENSO variability is characterized by means of the Niño3.4 index, defined in the region 170–120°W, 5°S–5°N (e.g., Trenberth 1997), and was obtained from http://www.cpc.ncep.noaa.gov/data/indices. The Niño3.4 index employed here is slightly different from that in Yu (2007), which used the index updated to 2001 from the Climate Analysis Section at NCAR. Figure 2a displays the timeseries of the PNA and Niño3.4 indices for DJF. For both indices, values above the threshold of one standard deviation are used to define anomalous events. Accordingly, we identify ten positive and seven negative PNA events, and 8 El Niño and 7 La Niña events for the period 1957/1958 to 2001/2002 (Table 1). The selected ENSO events are similar to those identified in previous studies (e.g., Trenberth 1997).

Table 1 List of DJF winters for PNA and Niño3.4 composites

+PNA	1958	1961	1964	1970	1977	1978	1981	1983	1986	1998
−PNA	1965	1969	1971	1972	1979	1982	1989			
+PNAa[a]	1961	1963	1964	1970	1977	1978	1981	1986		
−PNAa	1965	1966	1969	1972	1979	1982	1991	1993		
+Niño3.4	1958	1966	1973	1983	1987	1992	1995	1998		
−Niño3.4	1971	1974	1976	1985	1989	1999	2000			

Years are labeled on January of the DJF winters

[a] PNAa indicates the new index after removing the Niño3.4 contribution

Empirical orthogonal function (EOF) analysis is applied to the tropical Pacific interannual SST anomalies to represent the modeled ENSO variability, and to the Northern Hemisphere (20–90°N) sea-level pressure (SLP) anomalies to represent the modeled PNA variability, simulated by the CCCma coupled climate model. This is discussed further in Sect. 4.

2.2 Reanalysis and model data

Diagnoses are mainly based on the NCEP–NCAR reanalysis (Kistler et al., 2001) and the ECMWF ERA-40 reanalysis (Uppala et al. 2005) for the overlapping 45-year period from September 1957 to August 2002. These data are also referred to as "observations" in this analysis, although they are a combination of observations and model data. Both 6-hourly (00, 06, 12, and 18 UTC) and monthly mean isobaric fields were extracted on a 2.5° latitude–longitude global grid at 17 pressure levels (10, 20, 30, 50, 70, 100, 150, 200, 250, 300, 400, 500, 600, 700, 850, 925, and 1,000-hPa). The

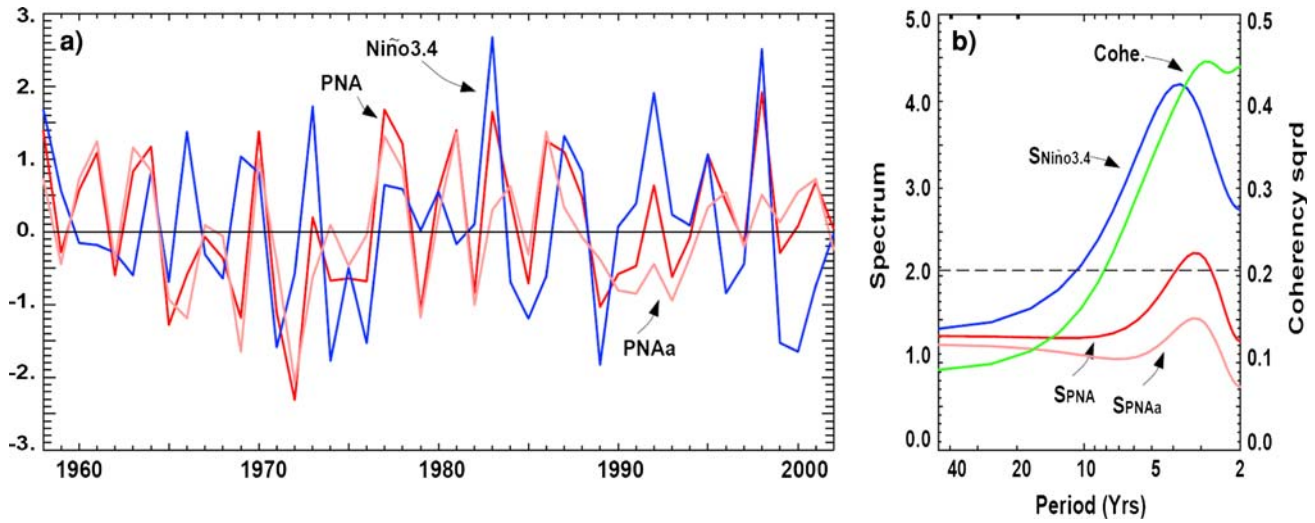

Fig. 2 **a** Time series of the normalized PNA (*red*), PNAa (*pink*), and Niño3.4 (*blue*) indices for DJF. **b** Spectra for the PNA, the PNAa, and Niño3.4 indices, and cross spectrum between the PNA and Niño3.4 indices. PNAa indicates the PNA index after removing the Niño3.4 contribution. *Dashed line* denotes the 5% level for the coherency squared for an uncorrelated process

variables considered include net shortwave and longwave radiation at the top of the atmosphere (TOA) and at the surface; surface latent and sensible heat fluxes; precipitation; and geopotential height, temperature and horizontal velocities in the troposphere. Anomalies are calculated relative to the 1961–1990 30-year climatology.

A 1,000-year integration of the first generation of the CCCma coupled climate model (CGCM1) is also analyzed in this study to confirm the observational results. As described in Flato et al. (2000), the atmospheric component of this coupled general circulation model is a spectral model with T32L10 triangular resolution. The oceanic component is a version of the GFDL MOM model (Pacanowski 1993) at a horizontal resolution of 1.8° × 1.8° and with 29 levels in the vertical. The coupled model and its control climate were described in Flato et al. (2000) and Boer et al. (2000). The model produces a realistic climate in terms of global patterns of mean SLP, surface air temperature, SST and salinity, precipitation, realistic-looking correlation patterns such as PNA and North Atlantic oscillation (NAO). However, modeled interannual variability in seasonal mean SLP is somewhat weaker than observed in the extratropical winter storm track regions (Fyfe et al. 1999) and modeled SST variability is weaker than observed, particularly in the eastern tropical Pacific (e.g., Yu and Boer 2002). The relatively weak temperature variability in the model is partially conditioned on the thickness (50 m) of the upper ocean layer provided that the forcing of SST by the modeled and observed atmosphere is similar (Yu and Boer 2006). Nevertheless, the ENSO associated tropical circulation, global SLP and geopotential height teleconnections are qualitatively similar to those observed (e.g., Flato et al. 2000). Therefore, we think it is appropriate to use this long climate simulation to examine the modeled PNA pattern with its associated diabatic heating and Rossby wave source anomalies to confirm the observational results. The variables considered include DJF winter monthly mean SLP, SST, geopotential height, precipitation, net shortwave and longwave radiation at the TOA, net shortwave and longwave radiation at the surface, and surface latent and sensible heat fluxes.

2.3 Diagnostic methods

Several thermodynamical and dynamical fields in association with the PNA pattern have been examined. We diagnose the atmospheric heating by examining both the three-dimensional net diabatic heating and the vertically integrated heating. We calculate the 3D diabatic heating of the atmosphere as a residual from the time-averaged thermodynamic equation (e.g., Hoskins et al. 1989; Nigam 1994). The vertically integrated total diabatic heating (e.g., Boer 1986; Trenberth and Solomon 1994) is calculated by using energy balance variables at the TOA and at the surface. We also diagnose the Rossby wave source at 200-hPa (e.g., Sardeshmukh and Hoskins 1988; Rasmusson and Mo 1993) to help understand the relationship between the upper-level divergence and the remote streamfunction response.

In addition, to isolate the ENSO related effect, we perform both partial correlation analysis and regression analysis. For three variables of y, $x1$ and $x2$, the partial correlation is defined as $r_{yx1,x2} = \frac{r_{yx1} - r_{yx2}\, r_{x1x2}}{\sqrt{(1-r_{yx2}^2)(1-r_{x1x2}^2)}}$, where $r_{yx1,x2}$ denotes the partial correlation of y and $x1$ with the contribution of $x2$ being extracted from both, while r_{yx} is the original correlation of two variables. If the original correlation is significant but the result is not for partial correlation, the original correlation is assumed as spurious, i.e. no direct causal link exists between y and $x1$. In this way, the independent contribution of $x1$ to y can be singled out (e.g., von Storch and Zwiers 1999; Wang et al. 2005). For composites, we remove ENSO signals in the PNA index and the fields of interest by means of regression analysis (e.g., Zhang et al. 1996). For the observational analysis, the ENSO signal is defined by the Niño3.4 index. Thus for the PNA index after removing the Niño3.4 contribution, denoted as PNAa and shown in Fig. 2, we identify eight positive and eight negative events during the analyzed period (Table 1). Statistical significance of the results is also estimated in this study.

3 Observational results

3.1 Relation between PNA and ENSO

Figure 2a shows the timeseries of the PNA and Niño3.4 indices for DJF mean from 1957/1958 to 2001/2002, along with the timeseries of the PNA index after removing the Niño3.4 contribution (PNAa). Both the PNA and Niño3.4 indices exhibit weak secular trends (not shown), while they are highly related with the correlation coefficient at 0.51 between the two original timeseries and at 0.52 between the timeseries after removing the corresponding secular trends, both are significant at greater than the 1% level after removing autocorrelation effects as in Leith (1973). This also indicates that the two indices have about 1/4 variations in common. Figure 2b further shows the spectrum and cross spectrum of the two indices. Both indices exhibit significant interannual variability (compared to the red-noise spectrum, not shown), consistent with previous studies (e.g., Feldstein 2000). The two indices are also found to co-vary significantly at the interannual timescales (period of 8–9 years or shorter), with power peak at around 3 years. The coherent phase illustrates that Niño3.4 leads the PNA slightly at these timescales (not shown),

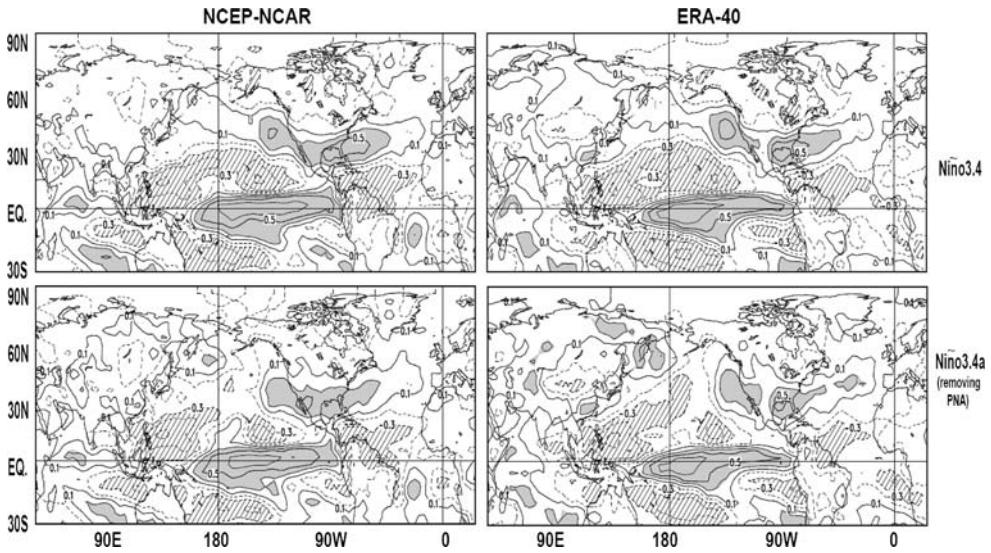

Fig. 3 Correlations of vertically integrated heating $\tilde{Q}$ with Niño3.4 index (*upper panels*) and with Niño3.4 index after removing the PNA contribution (*lower panels*). Results are obtained from the NCEP–NCAR reanalysis (*left column*) and from the ERA-40 reanalysis (*right column*). Contour interval is 0.2 (…, −0.3, −0.1, 0.1, …), with the zero contour omitted. The anomalies exceeding the 5% level *t* test are *shaded* (positive) and *hatched* (negative)

suggesting the potential influence of ENSO on the interannual variability of the PNA pattern, as reported in previous studies (e.g., Trenberth et al. 1998).

Figure 2b also shows the spectrum of the PNA after removing the Niño3.4 contribution by means of regression analysis. The powers of the PNA decrease 1/4–1/3 at the interannual timescales and change weakly at the decadal timescales after removing the ENSO component. Regressions of geopotential heights at 500-hPa including and excluding the ENSO component on the corresponding PNA indices exhibit similar features with a train of atmospheric waves, indicated by a sequence of high and low centers that extends from the tropical Pacific towards the North Pacific, North America and then the subtropical North Atlantic (not shown). Only modest differences in the values of the PNA centers of action are seen between the two regressions. Both the power spectrum and the regression analyses indicate that ENSO explains only some portion of the PNA variability.

We then examine the atmospheric diabatic heating and the Rossby wave source to help understand the forcing and wave source regions of the PNA pattern.

3.2 Vertically integrated diabatic heating

Following Boer (1986) and Trenberth and Solomon (1994), the vertically integrated total diabatic heating can be expressed as

$$\tilde{Q} = R_T - F_S + L(P - E), \quad (1)$$

where R_T is the downward radiation at TOA, F_S is the downward surface flux (including radiative and turbulent heat fluxes), $L = 2.5 \times 10^6$ J kg^{-1} is the latent heat due to evaporation, P is the precipitation rate, and E is the surface evapotranspiration. The vertically integrated heating is computed using monthly variables from both the NCEP–NCAR and ERA-40 reanalyses.

Figure 3 displays the geographical distributions of heating $\tilde{Q}$ correlated and partially correlated (removing the PNA effect) with ENSO. Figure 4 shows the similar quantities but for the correlations of heating $\tilde{Q}$ with the PNA and with the PNA after removing the Niño3.4 contribution. ENSO related heating is dominated by the tropical centers with the strongest heating in the equatorial central-eastern Pacific surrounded by cooling in the western Pacific, consistent with previous studies emphasizing the role from both positive and negative heating anomalies in the tropics (e.g., Wallace et al. 1992, 1998; DeWeaver and Nigam 2004). ENSO related heating changes very weakly when the PNA component is removed (Fig. 3, lower panels). The spatial correlations between the ENSO related heating patterns including and excluding the PNA component within the zonal band of 30°S–60°N are 0.93 and 0.94, respectively, for the NCEP–NCAR and the ERA-40 (Table 2). In addition, the ENSO related heating patterns bear close resemblance between the NCEP–NCAR and the ERA-40 reanalyses. One slight difference between the two appears in the equatorial eastern Pacific, with the strongest heating locating in the central-eastern Pacific for the NCEP–NCAR and shrinking somehow to the dateline for the ERA-40.

The PNA related heating, including the ENSO contribution (Fig. 4, upper panels), bears some resemblance to that of ENSO in the eastern Pacific. However, the

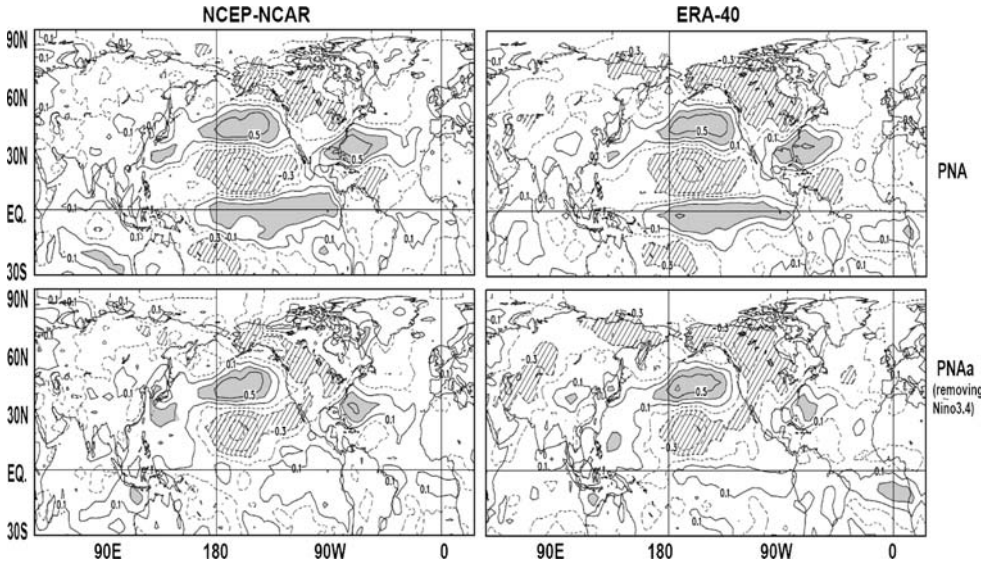

Fig. 4 As in Fig. 3, but for correlations of $\tilde{Q}$ with the PNA index (*upper panels*) and with the PNA index after removing the Niño3.4 contribution (*lower panels*)

Table 2 Spatial correlations within the zonal band of 30°S–60°N between the heating patterns (shown in Figs. 3 and 4) in association with different indices

	PNA	PNAa	Niño3.4	Niño3.4a
PNAa	0.77 (0.75)	1.0 (1.0)		
Niño3.4	0.74 (0.75)	0.15 (0.13)	1.0 (1.0)	
Niño3.4a	0.44 (0.48)	−0.21 (−0.21)	0.93 (0.94)	1.0 (1.0)

PNAa indicates the PNA index after removing the Niño3.4 contribution. Niño3.4a indicates Niño3.4 index after removing the PNA contribution. Results shown outside and inside the parentheses are based on the NCEP–NCAR and ERA-40 reanalyses, respectively

anomalies in the western Pacific are much weaker with respect to ENSO; meanwhile the centers over the North Pacific and the tropical Pacific are of comparable magnitudes. This indicates the major heating contribution to the PNA pattern lies in the eastern Pacific. On the other hand, in contrast to the ENSO related heating anomalies (Fig. 3), the correlations between the PNA and heating $\tilde{Q}$ differ markedly between the cases with and without the Niño3.4 contribution (Fig. 4, lower panels).

For both the NCEP–NCAR and the ERA-40, tropical anomalies are mostly reduced in the partial correlations, while anomalies elsewhere are only modestly affected. The spatial correlation coefficients between the PNA related heating patterns including and excluding the ENSO contribution within 30°S–60°N are 0.77 and 0.75, respectively, for the NCEP–NCAR and the ERA-40 (Table 2). The correlations are much lower than those between the ENSO related heating patterns with and without the PNA contribution (0.93–0.94) as noted above. Additionally, the ENSO related heating pattern correlates with the PNA related pattern at $\sim$0.75, but with the pattern associated with the PNA excluding the Niño3.4 contribution at only $\sim$0.15 (Table 2). This indicates that the PNA associated heating is confined outside the tropics when ENSO is removed, consistent with Yu (2007). The results from both reanalyses are very similar.

The insensitivity of the PNA pattern to tropical SST anomalies has been investigated numerically and observationally in previous studies (e.g., Simmons et al. 1983; Hoerling and Ting 1994; Zhang et al. 1996). On the other hand, it has been demonstrated that dynamical effects such as those from storm tracks play a significant role in the extratropical wave train (e.g., Hoerling and Ting 1994). The excitation of storm track eddies may be controlled by the baroclinicity of the low-level flow, which is strongly tied to the local thermal forcing (Hoskins and Valdes 1990; Held et al. 2002). Results from this analysis (cf. Fig. 4) further demonstrate the insensitivity of the PNA pattern to the tropical diabatic heating and suggest the independence of the PNA on ENSO variability in this regard, although the tropical forcing may act as an effective source of excitation for the pattern (e.g., Yu and Zwiers 2007).

Figure 5 shows composites of heating anomalies for the positive and negative PNA events, and their linear and nonlinear components. Here ENSO signals in both the PNA index and the heating field were removed by regression analysis. We estimate the linear and nonlinear components of the PNA related heating, respectively, as half difference and half summation of $\tilde{Q}$ anomalies of positive and negative composites (e.g., Hoerling et al. 1997). The heating anomalies for both polarities of the PNA bear a resemblance to the partial correlation pattern over the Pacific basin (cf. lower panels in Fig. 4). Accordingly, the linear component is marked by the anomalies with a dipole structure in the northern subtropics and mid-latitudes. These centers of action of heating

anomalies are significantly different from zero at the 5% level. Relatively weak patches of heating anomalies are also seen over mid-latitudes along the PNA path (e.g., Wallace and Gutzler 1981), downstream of the heating dipole over North America and the western North Atlantic. As would be expected, the precipitation related term (LP) dominates the heating anomalies (Fig. 6). The precipitation anomalies in the extratropics may be related to changes in large semi-permanent anticyclones, and particularly changes in the storm track (e.g., Peixoto and Oort 1992; Favre and Gershunov 2006). In addition, very good correspondence in the composites can be seen in the two reanalyses, but slight differences are seen in intensity detail. The heating anomalies with the ENSO contribution (not shown) from both the NCEP–NCAR and the ERA-40 show quite similar results in the subtropics and mid-latitudes, while stronger values are also seen in the tropics as expected and indicated above in Fig. 4.

The nonlinearity of heating anomalies mainly appears around the equator, with several patches of marginally significant centers close to the western and central Pacific (Fig. 5, lower panels). This is slightly different from that obtained in Yu (2007), which shows a tripole structure with heating anomalies in the eastern Indian Ocean, the western Pacific and the central Pacific. Nonetheless, as pointed out in that analysis, the centers around the western Pacific are only marginally significant at the 5% level. The patterns of the heating nonlinearity from the two reanalyses are broadly similar, the ERA-40 anomalies are relatively stronger in the tropics, especially around the equatorial dateline. The latter is partially due to the relatively stronger values of tropical precipitation in the ERA-40 as compared to the NCEP–NCAR, as seen in Fig. 1 and noted in previous studies (e.g., Trenberth et al. 2001).

The observational evidence, i.e. the feature of tropical heating anomalies (Fig. 5, lower panels), also bears some resemblance to early studies (e.g., Simmons et al., 1983) indicating that large perturbations over the North Pacific are most easily excited by forcing located over Southeast Asia and the tropical northwest Pacific Ocean, and to a recent study (Lin et al. 2005) indicating that a positive PNA is associated with the convective anomalies in the tropical western-central Pacific.

3.3 Vertical structure of heating anomalies

In the tropics, the thermodynamic balance is between diabatic heating and adiabatic cooling. The tropical circulation is hence closely linked to the vertical heating gradient. In contrast, heating at any level in mid-latitudes is mainly balanced by horizontal advection of temperature. Examination of vertical structure will be interesting to reveal the extent of differences of the PNA associated heating anomalies at different troposphere levels.

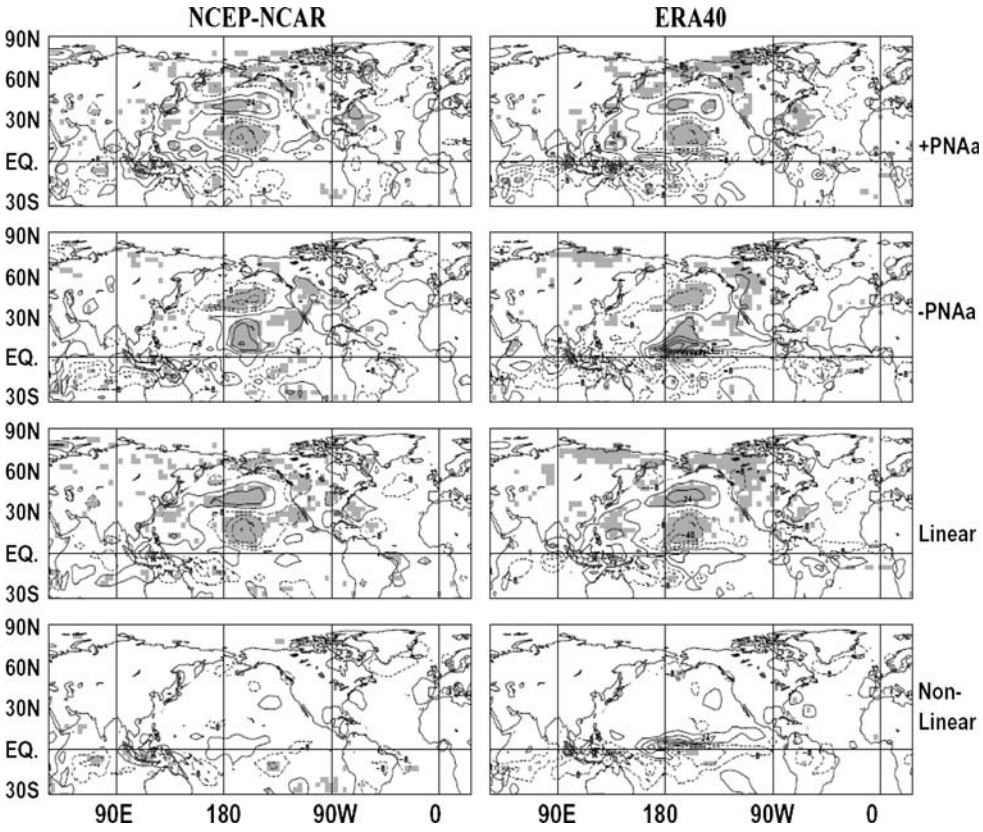

Fig. 5 Composites of $\tilde{Q}$ anomalies (removing the Niño3.4 contribution) for the positive PNA winters, the negative PNA winters, and their linear and nonlinear components, shown from the *top to the bottom*. Results are obtained from the NCEP–NCAR reanalysis (*left column*) and the ERA-40 reanalysis (*right column*). Contour interval is 16.0 W m^{-2} (…, −24.0, −8.0, 8.0, …), with the zero contour omitted. The anomalies that are significantly different from zero at the 5% level are *shaded*

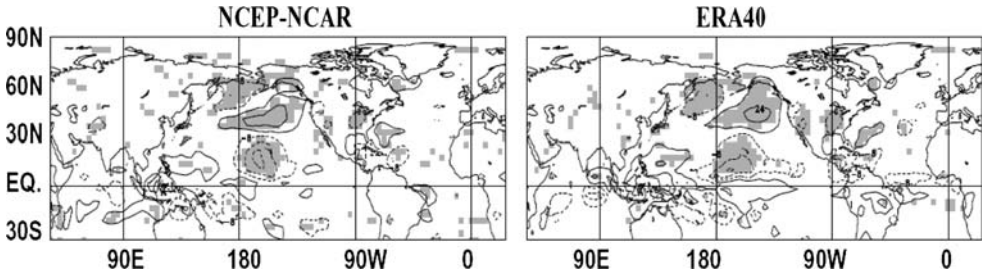

Fig. 6 Linear components of *LP* anomalies (removing the Niño3.4 contribution) from the NCEP–NCAR reanalysis (*left panel*) and the ERA-40 reanalysis (*right panel*). Contour interval is 16.0 Wm^{-2} (…, −24.0, −8.0, 8.0, …), with the zero contour omitted. The anomalies that are significantly different from zero at the 5% level are *shaded*

We calculate the three-dimensional diabatic heating Q as a residual from the time-averaged thermodynamic equation (e.g., Hoskins 1989; Nigam 1994) as follows,

$$Q = \frac{\Delta T}{\Delta t} + \overline{V} \cdot \nabla \overline{T} + (p/p_0)^{\kappa} \overline{\omega} \frac{\partial \overline{\theta}}{\partial p} + (p/p_0)^{\kappa} \left[\nabla \cdot \overline{V'\theta'} + \frac{\partial \left(\overline{\omega'\theta'} \right)}{\partial p} \right], \quad (2)$$

where T is the temperature, $\boldsymbol{V}$ *(u,v)* are the horizontal velocities, ω is the vertical velocity, θ is the potential temperature, and $\kappa = R/C_p = 0.286$. The overbar designates the monthly average and prime indicates the departure of the 6-h analysis from the monthly average. The diabatic heating includes contributions from the temperature tendency, a negligible term, the advection terms related to the mean state (terms 2 and 3 in Eq. 2) and the advections related to the eddy effect (term 4 in Eq. 2). The monthly 3D diabatic heating is calculated based on 6-hour isobaric fields from the NCEP–NCAR and ERA-40 reanalyses. In principle, the vertical integration of the 3D heating is equal to the total heating estimated above in Sect. 3.2. The consistency of heating results calculated from the two different approaches, as shown in the following, also severs to validate our results.

The robustness of the 3D diabatic heating calculation was established by comparing our results with those from previous studies. The seasonal and annual mean climatology of atmospheric diabatic heating calculated from the 45-year NCEP–NCAR and ERA-40 reanalyses resemble those from the ECMWF initialized analyses for March 1979–February 1989 (Hoskins 1989) and from the NCEP–NCAR reanalyses for a 15-year period from 1980 to 1994 (Yanai and Tomita 1998). Diabatic heating associated with ENSO also compares well with those reported in Nigam et al. (2000) from both the ECMWF and the NCEP–NCAR reanalyses during the overlapping 1979–1993 period.

Figure 7 displays the diabatic heating anomalies at 500-hPa (Q_{500}) and 925-hPa (Q_{925}) for the differences between the positive and negative PNA winters, after removing the ENSO contribution. The PNA related heating anomalies are generally dominated by a dipole structure over the northern Pacific with centers in mid-latitudes and the subtropics, particularly for the patterns at 500-hPa, consistent with that seen in the vertically integrated heating (Fig. 5). The centers of action of the heating anomalies are significantly different from zero at the 5% level. In addition, the heating anomalies are generally of comparable magnitudes at these two levels. However, the positive heating is more zonally oriented and only extends eastward to 160°W over the North Pacific at 925-hPa, different from the counterpart locating mainly over the northeast Pacific at 500-hPa. This indicates that the heating anomalies change sign with height

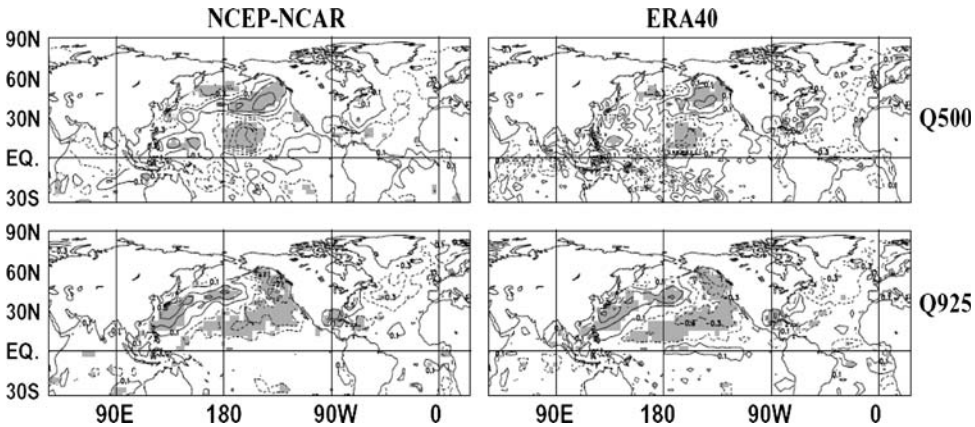

Fig. 7 Linear components of diabatic heating anomalies (removing the Niño3.4 contribution) over the oceans at 500-hPa (Q_{500}, *upper panels*) and at 925-hPa (Q_{925}, *lower panels*). Results are obtained from the NCEP–NCAR reanalysis (*left column*) and from the ERA-40 reanalysis (*right column*). Contour interval is 0.2 K/Day (…, −0.3, −0.1, 0.1, …), with the zero contour omitted. The anomalies that are significantly different from zero at the 5% level are *shaded*

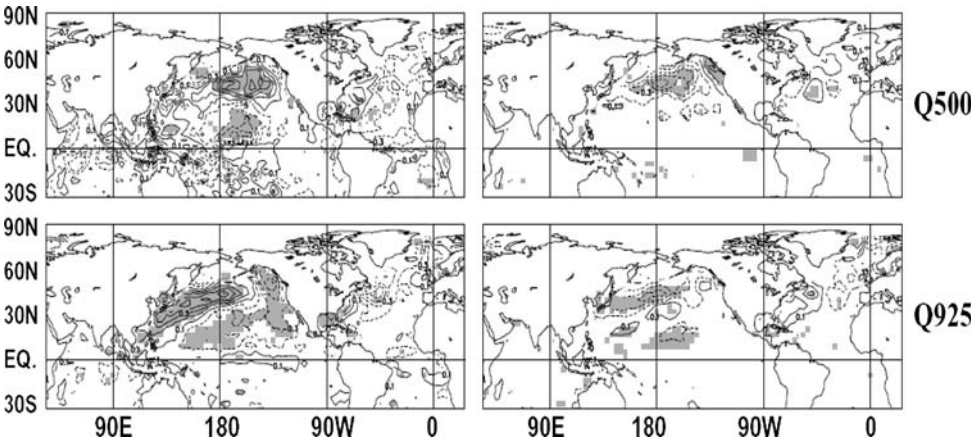

Fig. 8 Linear components of the advection terms of diabatic heating anomalies (removing the Niño3.4 contribution), related to the mean state (*left panels*) and the eddy effect (*right panels*), over the oceans at 500-hPa (*upper panels*) and at 925-hPa (*lower panels*). Results are obtained from the ERA-40 reanalysis. Contour interval is 0.2 K/Day (…, −0.3, −0.1, 0.1, …), with the zero contour omitted. The anomalies that are significantly different from zero at the 5% level are *shaded*

in the mid-latitudes of the eastern North Pacific. In addition, the PNA associated heating anomalies are largely supported by the advection terms related to the mean state and only partially damped by the eddy effect, especially in the North Pacific, for both Q_{500} and Q_{925} (Fig. 8). This is in accord with the canonically thermodynamic balance indicating that heating is balanced by horizontal advection of temperature in mid-latitudes (e.g., Hoskins and Karoly 1981).

Figure 9 presents the vertical structure of the PNA related heating anomalies in the central-eastern Pacific after removing the ENSO component. The heating anomalies that are significantly different from zero at the 5% level mainly appear in the northern subtropics and mid-latitudes as expected. By comparison, the anomalies are relatively weaker and mostly not significant around the equator. In the northern subtropics, the heating is characterized by deep

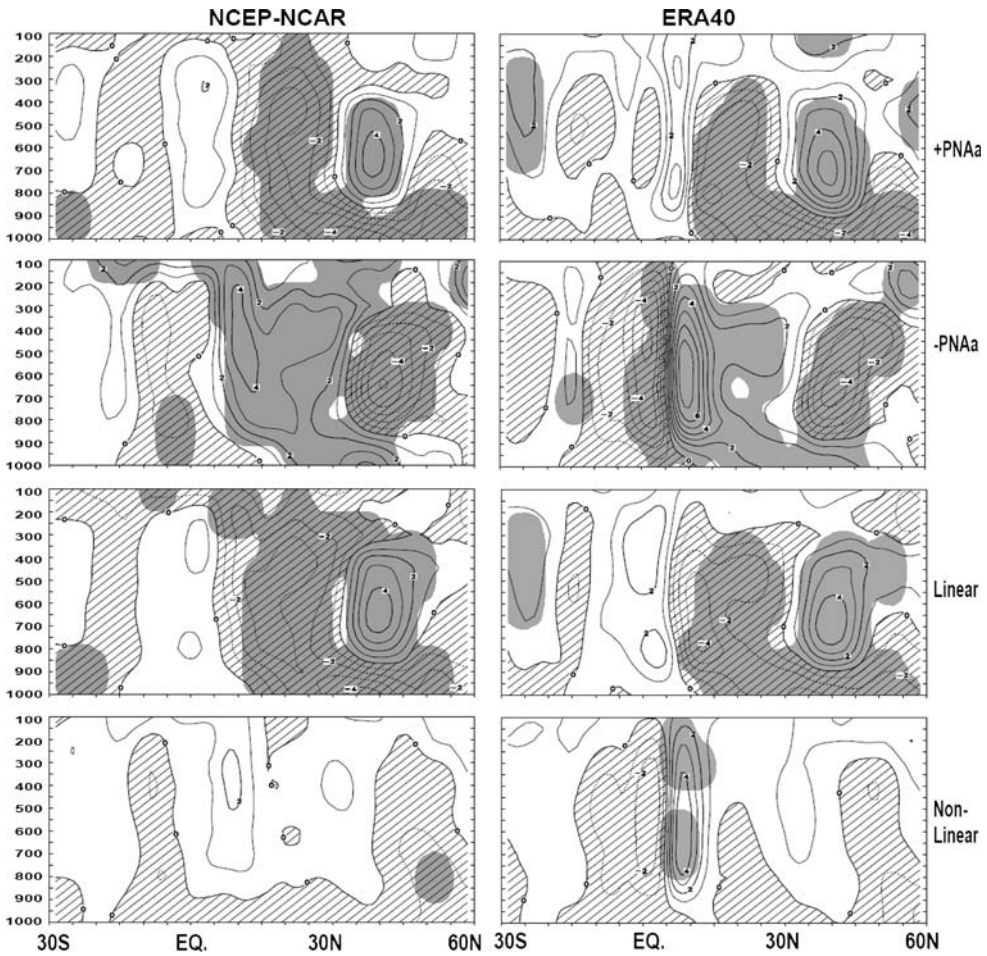

Fig. 9 Vertical structure of heating anomalies (removing the Niño3.4 contribution) in the central Pacific (180–120°W) for the positive PNA winters, the negative PNA winters, and their linear and nonlinear components, shown from the *top* to the *bottom*. Results are obtained from the NCEP–NCAR reanalysis (*left column*) and the ERA-40 reanalysis (*right column*). Contour interval is 1.0×10^{-1} K/Day. Negative values are *hatched*. The anomalies that are significantly different from zero at the 5% level are *shaded*

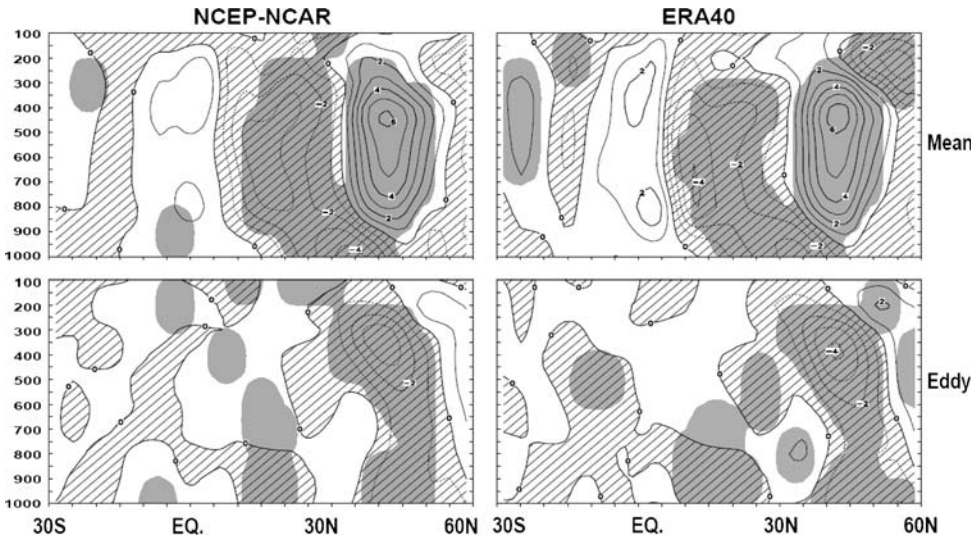

Fig. 10 Vertical structure of advection terms of heating anomalies (removing the Niño3.4 contribution), related to the mean state (*upper panels*) and the eddy effect (*lower panels*), in the central Pacific (180–120°W) for half differences between the positive and negative PNA winters. Results are obtained from the NCEP–NCAR reanalysis (*left column*) and the ERA-40 reanalysis (*right column*). Contour interval is 1.0×10^{-1} K/Day. Negative values are *hatched*. The anomalies that are significantly different from zero at the 5% level are *shaded*

anomalies with the same sign throughout the troposphere. In contrast, the heating switches sign with height in mid-latitudes, and is dominated by the anomalies in the middle troposphere. This is also consistent with the results in Yu (2007). Additionally, the results depend only weakly on the areas averaged in the central-eastern Pacific. The different vertical structures in the northern subtropics and mid-latitudes may be related to different diabatic heating scenarios, i.e. the shallow heating scenario of Hoskins and Karoly (1981) and the deep heating scenario of Palmer and Sun (1985). The heating structure over the northeast Pacific also bears some resemblance to that of the Antarctic Circumpolar Waves as reported recently by White and Chen (2002), although the thermodynamical mechanisms (such as the anomalous vorticity budget) have not been examined further in our study. In addition, the sources of anomalous diabatic heating remain to be investigated.

Broadly similar patterns are seen from the NCEP–NCAR and ERA-40 reanalyses. However, there is a relatively stronger meridional gradient of the heating in the northern subtropics for the ERA-40 with respect to the NCEP–NCAR, especially for the negative PNA winters. In addition, the anomalous heating centers appear in relatively lower troposphere for the ERA-40 compared to the NCEP–NCAR. The feature resembles that found from the ENSO related heating, which shows ECMWF heating to be considerably stronger than that of the NCEP–NCAR in the lower troposphere in the central equatorial Pacific (e.g., Nigam et al. 2000). Differences in the heating anomalies from the NCEP–NCAR and the ERA-40 may arise from several factors, including reanalysis model configuration, initialization scheme and convection parameterizations, which remain to be investigated.

The PNA related heating anomalies are largely supported by the advection related to the mean state throughout the troposphere (Fig. 10, upper panels), resembling those from the spatial patterns at Q_{500} and Q_{925} (Fig. 8). The eddy related advection (Fig. 10, lower panels) tends to damp the advection related to the mean state, especially at the upper troposphere over the North Pacific.

The PNA related heating anomalies (removing the ENSO contribution) are relatively weaker along the equator with respect to those in the northern subtropics and mid-latitudes over the central Pacific, especially for the heating away from the western-central Pacific (Fig. 11). The tropical heating anomalies generally extend deep in the troposphere, in particular for the ERA-40 reanalysis. This is probably related to the convective thermodynamic balance between diabatic heating and adiabatic cooling in the tropics. It is also noted that the linear and nonlinear components of the heating anomalies are of comparable magnitudes along the equator, especially for those near the dateline. This is different from Yu (2007) indicating that the nonlinearity dominates the PNA related tropical heating, particularly for the heating near the maritime continent. The difference may be due to variations in association with different samples used in the two studies. Nonetheless, only several patches of the equatorial centers are significantly different from zero, as seen here for both reanalyses and in the previous study (Fig. 5 of Yu 2007).

3.4 Rossby wave source anomalies

The PNA teleconnection pattern is well defined at middle and upper troposphere levels, and is characterized by an equivalent barotropic structure (e.g., Wallace and Gutzler 1981; Simmons et al. 1983). The barotropic vorticity equation, linearized about an upper tropospheric zonal flow, can yield quite realistic tropospheric stationary wave anomalies including the observed PNA pattern (e.g.,

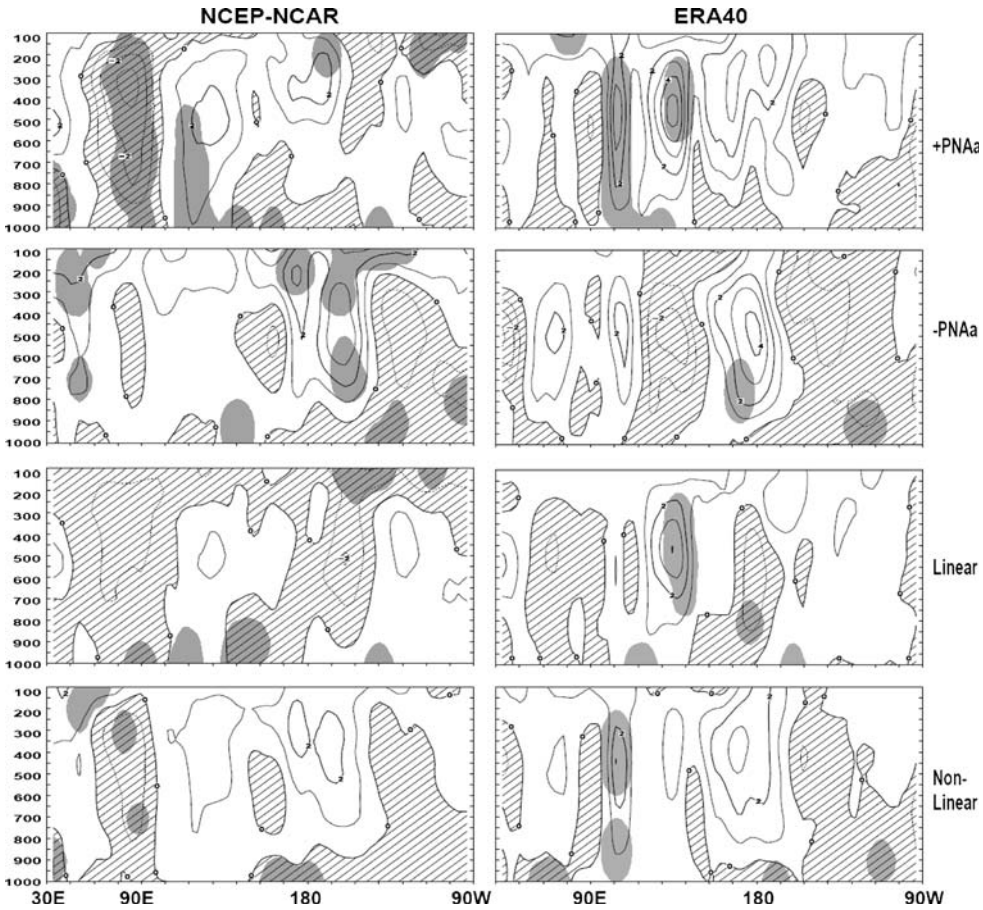

Fig. 11 Vertical structure of heating anomalies (removing the Niño3.4 contribution) along 10°S–10°N tropical band for the positive PNA winters, the negative PNA winters, and their linear and nonlinear components, shown from the *top* to the *bottom*. Results are obtained from the NCEP–NCAR reanalysis (*left column*) and the ERA-40 reanalysis (*right column*). Contour interval is 1.0×10^{-1} K/Day. Negative values are *hatched*. The anomalies that are significantly different from zero at the 5% level are *shaded*

Hoskins and Karoly 1981; Hoskins and Ambrizzi 1993). In particular, the upper-level divergence in the subtropics may result in a Rossby wave source that drives the rotational wind field and acts as an efficient generator of stationary Rossby waves. Sardeshmukh and Hoskins (1988) employed a barotropic vorticity model to diagnose the relationship between the upper-level divergence and the remote streamfunction response associated with a localized region of tropical heating. Following their study, the Rossby wave source (S) takes the following form,

$$S = -V_\chi \cdot \nabla(\zeta + f) - (\zeta + f)\nabla \cdot V_\chi = -\nabla \cdot \left[(\zeta + f)V_\chi\right], \tag{3}$$

where $\boldsymbol{V_\chi}$ represents the horizontally divergent wind velocity and is defined as the negative gradient of velocity potential χ. Here χ is obtained by solving the Poisson equation globally with divergence as the forcing term. ζ is the relative vorticity, and f is the Coriolis parameter. The Rossby wave source includes contributions from both the vortex stretching term and the advection of absolute vorticity by the divergent part of the flow. We examine Rossby wave sources at 200-hPa (S_{200}) in association with the PNA pattern in this study.

Figure 12 displays the composites of S_{200} anomalies for the positive and negative PNA events, and their linear and nonlinear components, with the ENSO contribution included. A train of wave forcing anomalies over the PNA sector dominates the S_{200} patterns. For positive (negative) PNA winters, the forcing anomalies are characterized by the strongest anticyclonic (cyclonic) wave forcing occurring over the eastern North Pacific, with cyclonic (anticyclonic) forcing occurring both upstream over the western and southern portions of the North Pacific and downstream over North America, and with another pair of positive and negative forcing anomalies over the subtropical western North Atlantic. The anomalies feature a PNA-like wave forcing, while no forcing sources are seen in the tropics. Only slight differences of the intensity of centers of action of S_{200} anomalies appear between the NCEP–NCAR and the ERA-40. The wave activity source is also collocated somewhat with the atmospheric diabatic forcing in the mid-high latitudes over the PNA sector (cf. Fig. 12 to Figs. 4 and 5), but is not consistent with the tropical forcing (Fig. 4, upper panels). In addition, the linearity dominates the PNA related Rossby wave sources. The centers of action of S_{200} anomalies are significantly different from zero at the 5% level for the linear component, while there is only a weak and not significant forcing band over the extratropical North Pacific for the nonlinear component.

The major feature of S_{200} anomalies over the PNA sector also bears some resemblance to the observational evidence of Rossby wave anomalies associated with the 1987–1989 ENSO cycle, which exhibits that Rossby wave source anomalies appear mainly in the extratropical North Pacific (Rasmusson and Mo 1993). However, in contrast to the 1987–1989 ENSO cycle, the PNA related wave forcing is also clearly evident in the subtropical North Pacific, with about 1/3–1/2 times the amplitude of those in the extratropical North Pacific. The anomalous wave sources in the North Pacific also collocate with the extratropical cyclone/anticyclone activity (e.g., Hoskins and Hodges 2002; Wernli and Schwierz, 2006), which is found to be closely related to air temperature in western North America (Favre and Gershunov 2006).

We also analyzed the similar quantities of Fig. 12, but excluding the ENSO contribution. The S_{200} anomalies for the positive and negative PNA winters and for their linear and nonlinear components remain virtually unchanged when the ENSO contribution is removed (not shown). As noted by Sardeshmukh and Hoskins (1985, 1988), it is conceivable that an alteration of the local Hadley circulation by the tropical forcing may have effectively migrated the stationary wave source from the tropics to the subtropics. On the other hand, while examining the causes of the 1988 drought over North America, Trenberth et al. (1988) have suggested that the anomalous flow pattern was primarily forced by diabatic heating related to warmer than normal SSTs in the subtropical Pacific. The similarity of the PNA related Rossby wave sources, obtained from the cases either with or without the ENSO contribution, demonstrates potential wave forcing in the North Pacific, regardless of tropical heating. However, dynamical processes, such as the PNA related variations of momentum fluxes by high-frequency eddies and its relationship to the diabatic heating anomalies, merit further study.

4 Modeling evidence

In this section, we analyze the modeled PNA pattern and its associated vertically integrated diabatic heating and Rossby wave source anomalies to confirm the observational results described above.

The modeled ENSO variability is represented by the first EOF of the tropical Pacific interannual SST variability as discussed in Yu and Zwiers (2007). The EOF analysis is performed for the tropical Pacific region bounded by 20°S–20°N and 120°E–70°W, and is applied to the DJF winter mean SST anomalies with bandpass filtering to retain periods between 2 and 8 years. The first EOF accounts for 27.3% of the total variance, and is well separated from subsequent EOFs as per the criterion of North et al. (1982). Figure 13a displays the SST anomalies over the Pacific

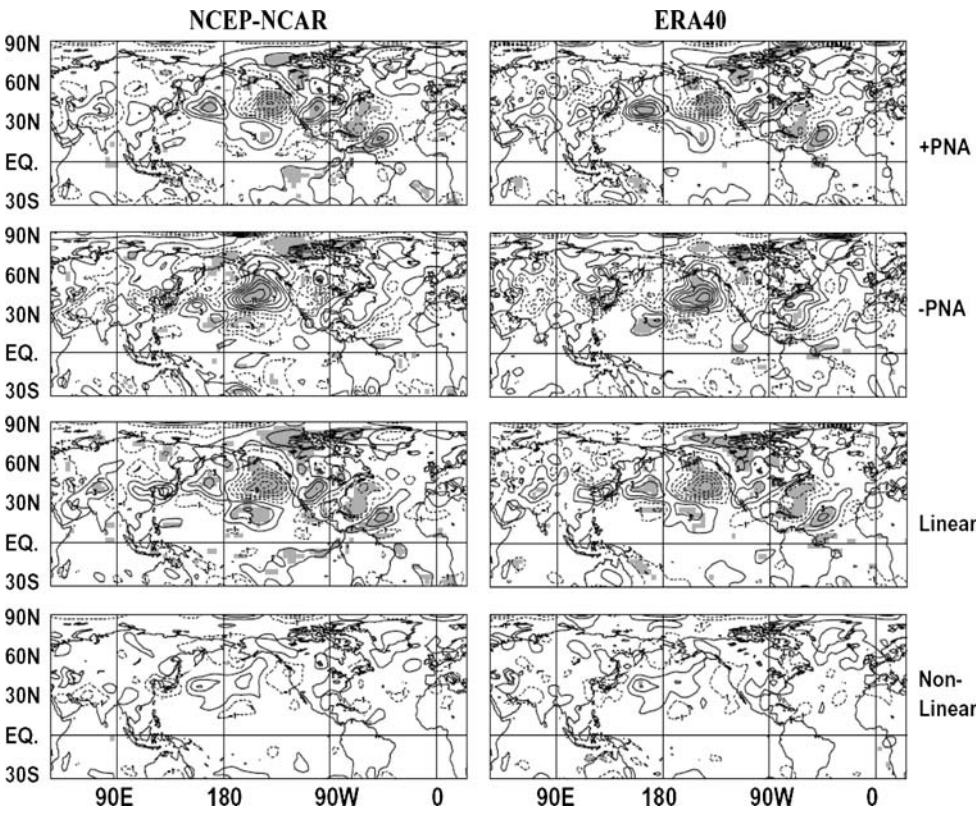

Fig. 12 Composites of anomalies of Rossby wave sources at 200-hPa (S_{200}, with the Niño3.4 contribution) for the positive PNA winters, the negative PNA winters, and their linear and nonlinear components, shown from the *top* to the *bottom*. Results are obtained from the NCEP–NCAR reanalysis (*left column*) and the ERA-40 reanalysis (*right column*). Contour interval is 2.0×10^{-11} s^{-2} (…, -3.0×10^{-11}, -1.0×10^{-11}, 1.0×10^{-11}, …), with the zero contour omitted. The anomalies that are significantly different from zero at the 5% level are *shaded*

basin regressed upon the normalized leading principal component (PC) timeseries of the modeled ENSO. The simulated SST mode has features similar to those typical features of an El Niño, with the strongest anomalies in the tropical central-eastern Pacific and weaker anomalies of opposite sign in the far western North and South Pacific. However, the tropical center of action shifts westward compared to the corresponding results from observations (e.g., Zhang et al. 1996). Current coupled climate models show a rather wide range of tropical temperature variability in both intensity and geographical distribution (e.g., Davey et al. 2002; Collins et al. 2005). There is no obvious factor or factors that govern this behavior in models. The physical process associated with the ENSO variability for this coupled climate model was reported in Yu and Boer (2002).

The modeled PNA index is represented by the timeseries associated with EOF2 of Northern Hemisphere (20–90°N) winter mean SLP anomalies. The EOF2 explains 11.7% of the total variance. This is another representation of the PNA as employed in some previous studies (e.g., http://jisao.washington.edu/data_sets/pna; Straus and Shukla 2002; Teng et al. 2007 for this coupled model). Figure 13b shows the geopotential height at 500-hPa regressed upon the normalized PC2 of Northern Hemisphere SLP anomalies. The modeled PNA is characterized by the strongest anomalies occurring over the North Pacific, with anomalies of opposite sign both upstream over the tropical central Pacific and downstream over North America, and with anomalies of the same sign over the subtropical North Atlantic. This simulated pattern generally resembles the observed patterns obtained by connecting the hemispheric geopotential height with various PNA related indices (e.g., Horel and Wallace 1981; Zhang et al. 1996).

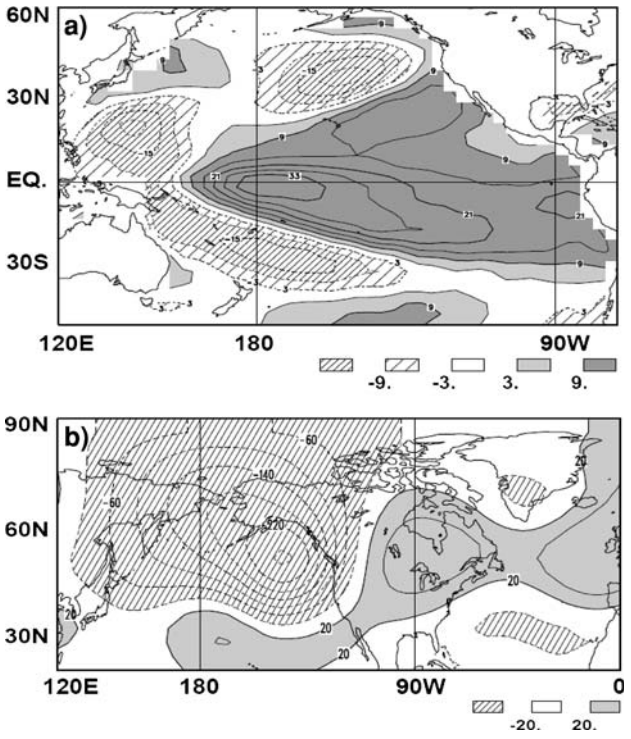

Fig. 13 (a) Regression pattern of SST over the Pacific basin (*upper panel*) on the normalized leading PC1 of 2-8-year bandpass filtered SST over the tropical Pacific (20°S–20°N, 120°E–70°W). Contour interval is 6.0×10^{-2} K per standard deviation of the related PC1 timeseries (…, -9.0×10^{-2}, -3.0×10^{-2}, 3.0×10^{-2}, …), with the zero contour omitted. (b) Regression pattern of geopotential height at 500-hPa (*lower panel*) on the normalized timeseries of the EOF2 of Northern Hemisphere (20–90°N) winter mean SLP anomalies. Contour interval is 40.0 m^2 s^{-2} per standard deviation of the related PC2 timeseries (…, −60.0, −20.0, 20.0, …), with the zero contour omitted

Figures 14a and b display the spatial distributions of vertically integrated heating $\tilde{Q}$ regressed upon the modeled PNA variability, with and without the modeled ENSO contribution, respectively. Figure 15 shows the same quantities for the Rossby wave source at 200-hPa. Regression results are presented here instead of correlations because they highlight large values and the anomalies significantly different from zero, and neglect small values mainly over lands in the eastern hemisphere, which are not significantly different from zero but overemphasized in correlations. With the modeled ENSO component, the PNA related heating is dominated by the anomalies both in the tropical Pacific and in the mid-high latitude North Pacific. These centers of action are of comparable magnitudes and are significantly different from zero at the 5% level. Relatively weak but

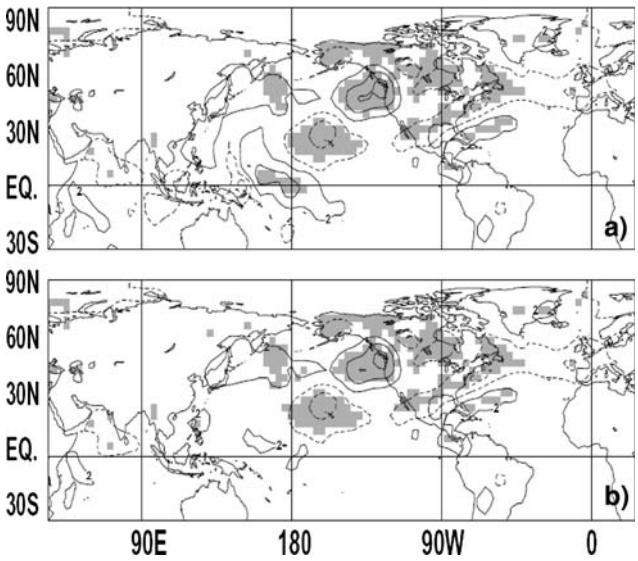

Fig. 14 Regression patterns of modeled vertically integrated $\tilde{Q}$ anomalies on the modeled PNA pattern for the cases with the modeled ENSO contribution (*upper panel*) and without the modeled ENSO contribution (*lower panel*). Contour interval is 4.0 Wm^{-2} per standard deviation of the modeled PNA index (…, −6.0, −2.0, 2.0, …), with the zero contour omitted. The anomalies that are significantly different from zero at the 5% level are *shaded*

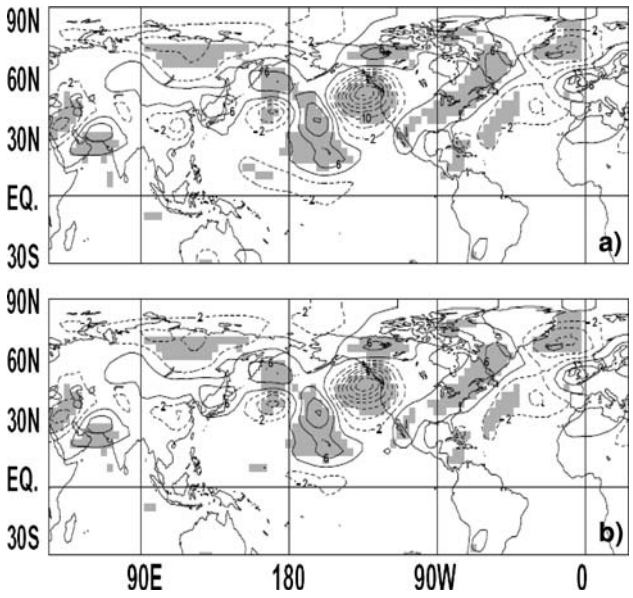

Fig. 15 As in Fig. 14, but for Rossby wave sources at 200-hPa (S_{200}). Contour interval is 4.0×10^{-12} s^{-2} per standard deviation of the modeled PNA index (…, -6.0×10^{-12}, -2.0×10^{-12}, 2.0×10^{-12}, …), with the zero contour omitted

significant anomalies are also seen downstream over North America and over the subtropical North Atlantic. The modeled heating pattern compares reasonably well with those obtained from the NCEP–NCAR and ERA-40 reanalyses (Fig. 4), although the modeled center of action in the tropics shifts westward with respect to the corresponding observations, as does in the SST field. We then removed the ENSO contribution in both the PNA and heating $\tilde{Q}$ field and recalculated the regression pattern. Consistent with the observation, tropical signals mostly diminish, while anomalies elsewhere are only modestly affected (Fig. 14b). This indicates that the PNA associated heating is confined outside the tropics, and confirms the observational results derived above. On the other hand, the Rossby wave source anomalies in association with the PNA pattern change very weakly between the cases either with or without the ENSO contribution (Fig. 15). This is also in agreement with the observations and suggests the effects of wave forcing sources in the mid-high latitudes on the PNA pattern.

The modeling analysis, based on 1,000-year of model output, increases confidence in observational results derived from the 45-year reanalyses.

5 Summary

The PNA and ENSO variability co-vary significantly at interannual timescales, with Niño3.4 index leading the PNA index slightly at these timescales. In general, ENSO explains about 1/4 of the PNA variability. The PNA related atmospheric diabatic heating is examined using the overlapping 45-year, period spanning September 1957–August 2002, NCEP–NCAR and ERA-40 reanalysis datasets, along with a 1,000-year long integration of the Canadian Center for Climate Modelling and Analysis coupled climate model. We analyze the PNA associated heating by linearly isolating the influence of ENSO, and examine both the vertically integrated and three-dimensional diabatic heating fields. We also diagnose the Rossby wave source in association with the PNA.

The PNA-related heating is dominated by anomalies in the eastern Pacific, a north–south dipole structure with the heating anomalies changing sign with height in mid-latitudes and having the same sign throughout the troposphere in the northern subtropics. Relatively weak heating anomalies are also seen over mid-latitudes along the PNA path, downstream of the dipole heating over North America and the western North Atlantic. Conversely, the PNA associated heating is rather weak in the tropics, remarkably different from that related to ENSO variability. These are consistent with the results reported in Yu (2007). The PNA heating anomalies are largely supported by the advection related to the mean state throughout the troposphere, and partially damped by the eddy related advection, particularly at the upper troposphere over the North Pacific.

Broadly similar patterns are seen from the NCEP–NCAR and ERA-40 reanalyses. Nevertheless, the anomalous heating centers are usually located at relatively lower troposphere for the ERA-40 with respect to the NCEP–NCAR, resembling those found for the ENSO-related heating (e.g., Nigam et al. 2000). Reasons for differences in the heating anomalies between the NCEP–NCAR and the ERA-40 remain to be studied.

The linear and nonlinear components of the PNA related heating are also estimated, following Hoerling et al. 1997, as half difference and half summation of heating anomalies of positive and negative composites, respectively. The linear component accounts for the majority of the PNA related heating anomalies, particularly in the mid-high latitudes. The nonlinearity of heating anomalies mainly appears around the equator, with several patches of marginally significant centers close to the western and central Pacific. This is slightly different from that noted in Yu (2007), which exhibits a tripole structure with heating anomalies in the eastern Indian Ocean, the western Pacific and the central Pacific. Nonetheless, only several patches of the equatorial centers are significantly different from zero, as seen in both analyses.

The PNA-related Rossby wave source exhibits a train of forcing anomalies, featured by a sequence of cyclonic and anticyclonic centers that extends from North Pacific towards North America and the subtropical North Atlantic, a PNA-like forcing pattern in mid-high latitudes. There is

no PNA related forcing source in the tropics. The wave activity source also collocates somewhat with the atmospheric diabatic forcing in the mid-high latitudes over the PNA sector. The results suggest the potential dynamical effect with local thermal forcing for the extratropical wave train.

The modeled PNA related heating is also confined outside the tropics, and compares reasonably well with those obtained from the observations, although the modeled center of action in the tropics shifts westward with respect to the observational counterpart. Modeling results also indicate the effects of wave forcing sources in the mid-high latitudes on the PNA pattern. The 1,000-year modeling analysis increases confidence in observational results derived from the 45-year reanalyses.

Acknowledgments We greatly appreciate the work of G.J. Boer, G.M. Flato, D. Ramsden, C. Reader, W. Lee, and other colleagues at the CCCma in the production of the model results analyzed here. We thank B. Merryfield and Q. Teng for helpful comments on this study, and A. Krol for editing the manuscript. In addition, we would like to thank two anonymous reviewers for their constructive suggestions and advice, which considerably improved the original manuscript.

References

Bengtsson L, Hagemann S, Hodges KI (2004) Can climate trends be calculated from reanalysis data? J Geophys Res 109, D11111. doi:10.1029/2004JD004536

Boer GJ (1986) A comparison of mass and energy budgets from two FGGE datasets and a GCM. Mon Wea Rev 114:885–902

Boer GJ, Flato G, Reader MC, Ramsden D (2000) A transient climate change simulation with greenhouse gas and aerosol forcing: experimental design and comparison with the instrumental record for the 20th century. Clim Dyn 16:405–425

Collins M, Sperber K, CMIP Modelling groups (2005) El Niño- or La Niña-like climate change? Clim Dyn 24:89–104

Davey M et al (2002) STOIC: a study of coupled model climatology and variability in tropical ocean regions. Clim Dyn 18:403–420

Deser C, Blackmon ML (1995) On the relationship between tropical and North Pacific sea surface temperature variations. J Clim 8:1677–1680

Deweaver E, Nigam S (2004) On the forcing of ENSO teleconnections by anomalous heating and cooling. J Clim 17:3225–3235

Favre A, Gershunov A (2006) Extra-tropical cyclonic/anticyclonic activity in North-Eastern Pacific and air temperature extremes in Western North America. Clim Dyn 26:617–629

Feldstein SB (2000) The timescale, power spectra, and climate noise properties of teleconnection patterns. J Clim 13:4430–4440

Flato GM, Boer GJ, Lee W, McFarlane N, Ramsden D, Reader M, Weaver A (2000) The Canadian Centre for Climate Modelling and Analysis global coupled model and its climate. Clim Dyn 16:451–467

Fyfe JC, Boer GJ, Flato GM (1999) The Arctic and Antarctic oscillations and their projected changes under global warming. Geophys Res Lett 26:1601–1604

Graham NE (1994) Decadal-scale climate variability in the tropical and North Pacific during the 1970s and 1980s: observations and model results. Clim Dyn 10:135–162

Hartmann D (1995) A PV view of zonal flow vacillation. J Atmos Sci 52:2561–2576

Held IM, Ting M, Wang H (2002) Northern winter stationary waves: theory and modeling. J Clim 15:2125–2144

Hoerling MP, Ting M (1994) Organization of extratropical transients during El Niño. J Clim 7:945–966

Hoerling MP, Kumar A, Zhong M (1997) El Niño, La Niña, and the nonlinearity of their teleconnections. J Clim 10:1769–1786

Horel JD, Wallace JM (1981) Planetary-scale atmospheric phenomena associated with the Southern Oscillation. Mon Wea Rev 109:813–829

Hoskins BJ, Ambrizzi T (1993) Rossby wave propagation on a realistic longitudinally varying flow. J Atmos Sci 50:1661–1671

Hoskins BJ, Hodges KI (2002) New perspectives on the Northern Hemisphere winter storm tracks. J Atmos Sci 59:1041–1061

Hoskins BJ, Karoly D (1981) The steady linear response of a spherical atmosphere to thermal and orographic forcing. J Atmos Sci 38:1179–1196

Hoskins BJ, Valdes PJ (1990) On the exsistence of storm-tracks. J Atmos Sci 47:1854–1864

Hoskins, B. J., H. H. Hsu, I. N. James, M. Masutani, P. D. Sardeshmukh, and G. H. White, (1989) Diagnostics of the global atmospheric circulation based on ECMWF analyses 1979–1989. Tech. document WCRP-27, WMO/TD-no. 326, WMO, 217 pp

Kistler R et al (2001) The NCEP–NCAR 50-year reanalysis: monthly means CD-ROM and documentation. Bull Am Meteor Soc 82:247–268

Lau N-C (1997) Interactions between global SST anomalies and the midlatitude atmospheric circulation. Bull Am Meteor Soc 78:21–33

Leith CE (1973) The standard error of time-average estimates of climatic means. J Appl Meteorol 12:1066–1069

Lin H, Derome J, Brunet G (2005) Tropical Pacific link to the two dominant patterns of atmospheric variability. Geophys Res Lett 32, L03801. doi:10.1029/2004GL021495

Nigam S (1994) On the dynamical basis for the Asian summer monsoon rainfall—El Niño relationship. J Climate 7:1750–1771

Nigam S, Chung C, DeWeaver E (2000) ENSO diabatic heating in ECMWF and NCEP–NCAR reanalyses, and NCAR CCM3 simulation. J Clim 13:3152–3171

Nitta T, Yamada S (1989) Recent warming of tropical sea surface temperature and its relationship to the Northern Hemisphere circulation. J Meteor Soc Jpn 67:375–382

North GR, Bell TL, Cahalan RF, Moeng FJ (1982) Sampling errors in the estimation of empirical orthogonal functions. Mon Wea Rev 110:699–706

Pacanowski RC, Dixon K, Rosati A (1993) The GFDL modular ocean model users guide. GFDL Ocean group technical report 2. GFDL, Princeton, USA, 46 pp

Palmer TN (1999) A nonlinear dynamical perspective on climate prediction. J Clim 12:575–591

Palmer T, Sun Z (1985) A modelling and observational study of the relationship between sea surface temperature in the northwest Atlantic and atmospheric general circulation. Q J R Meteor Soc 111:947–975

Peixoto J, Oort A (1992) The physics of climate, AIP, NY, 520 pp

Rasmusson EM, Mo K (1993) Linkages between 200-mb tropical and extratropical circulation anomalies during the 1986–1989 ENSO cycle. J Clim 6:595–616

Renwick JA, Wallace JM (1996) Relationships between North Pacific wintertime blocking, El Niño, and the PNA pattern. Mon Wea Rev 124:2071–2076

Sardeshmukh PD (1993) The baroclinic problem and its application to the diagnosis of atmospheric heating rates. J Atmos Sci 50:1099–1112

Sardeshmukh PD, Hoskins BJ (1985) Vorticity balances in the tropics during the 1982–93 El Nino-Southern oscillation event. Q J R Meteor Soc 111:261–278

Sardeshmukh PD, Hoskins BJ (1988) The generation of global rotational flow by steady idealized tropical divergence. J Atmos Sci 45:1228–1251

Simmons AJ, Wallace JM, Branstator GW (1983) Barotropic wave propagation and instability, and atmospheric teleconnection patterns. J Atmos Si 40:1363–1392

Straus DM, Shukla J (2002) Does ENSO force the PNA? J Clim 15:2340–2358

Teng Q, Fyfe JC, Monahan AH (2007) Northern hemisphere circulation regimes: observed, simulated and predicted. Clim Dyn 28:867–879

Trenberth KE (1997) The definition of El Niño. Bull Am Meteor Soc 78:2771–2777

Trenberth KE, Solomon A (1994) The global heat balance: heat transports in the atmosphere and ocean. Clim Dyn 10:107–134

Trenberth KE, Barnstator GW, Arkin PA (1988) Origins of the 1988 North American drought. Science 242:1640–1645

Trenberth KE, Branstator GW, Karoly D, Kumar A, Lau NC, Ropelewski C (1998) Progress during TOGA in understanding and modeling global teleconnections associated with tropical sea surface temperatures. J Geophys Res 103:14291–14324

Trenberth KE, Hurrell JW (1994) Decadal atmosphere-ocean variations in the Pacific. Clim Dyn 9:303–319

Trenberth KE, Stepaniak DP, Hurrell JW, Fiorino M (2001) Quality of reanalyses in the tropics. J Clim 14:1499–1510

Uppala SM et al (2005) The ERA-40 re-analysis. Q J R Meteor Soc 131:2961–3012

von Storch H, Zwiers FW (1999) Statistical analysis in climate research. Cambridge University Press, Cambridge, 494 pp

Wallace JM, Gutzler DS (1981) Teleconnections in the geopotential height field during the northern hemisphere winter. Mon Wea Rev 109:784–812

Wallace JM, Smith C, Bretherton CS (1992) Singular value decomposition of wintertime sea surface temperature 500-mb height anomalies. J Clim 5:561–576

Wallace JM, Rasmusson EM, Mitchell TP, Kousky VE, Sarachik ES, von Storch H (1998) On the tructure and evolution of ENSO-related climate variability in the tropical Pacific: lessons from TOGA. J Geophys Res 103:14241–14259

Wang D, Wang C, Yang X, Lu J (2005) Winter Northern Hemisphere surface air temperature variability associated with the Arctic Oscillation and North Atlantic Oscillation. Geophys Res Lett 32, L16706. doi:10.1029/2005GL022952

WCRP (2000) Intercomparison and validation of ocean-atmosphere energy flux fields. WCRP-112, WMO/TD-no. 1036, 303 pp

Wernli H, Schwierz C (2006) Surface cyclones in the ERA-40 dataset (1958–2001). Part I: Novel identification method and global climatology. J Atmos Sci 63:2486–2507

White WB, Chen SC (2002) Thermodynamic mechanisms responsible for the tropospheric response to SST anomalies in the Antarctic circumpolar pages. J Clim 15:2577–2596

Yanai M, Tomita T (1998) Seasonal and interannual variations of atmospheric heat sources and moisture sinks as determined from NCEP–NCAR reanalysis. J Clim 11:463–482

Yu B, Boer GJ (2002) The roles of radiation and dynamical processes in the El Niño-like response to global warming. Clim Dyn 19:539–553

Yu B, Boer GJ (2006) The variance of sea surface temperature and projected changes with global warming. Clim Dyn 26:801–821

Yu B, Zwiers F (2007) The impact of combined ENSO and PDO on the PNA climate: a 1000-year climate modeling study. Clim Dyn 29:837–851

Yu B (2007) PNA associated diabatic heating and its relationship to ENSO. Atmos Sci Lett 8:107–112

Zhang Y, Wallace JM, Iwasaka N (1996) Is climate variability over the North Pacific a linear response to ENSO? J Clim 9:1468–1478

Zwiers FW (1987) A potential predictability study conducted with an atmospheric general circulation model. Mon Wea Rev 115:2957–2974